Powder Technology 432 (2024) 119153

Contents lists available at ScienceDirect

Powder Technology

journal homepage: www.journals.elsevier.com/powder-technology

Development of an ultrasonically excited recoating process in laser powder bed fusion to process non-spreadable 316L powder

Kai Drechsel [a,*], Victor Lubkowitz [a], Lena Albrecht [a], Paul Schäfer [a], Markus Schneider [b], Volker Schulze [a], Frederik Zanger [a]

[a] wbk - Institute of Production Science, Kaiserstraße 12, Karlsruhe, 76133, Baden Württemberg, Germany
[b] PP-Tech Components GmbH, Ferdinand-Porsche-Straße 9, Ettlingen, 76275, Baden Württemberg, Germany

GRAPHICAL ABSTRACT

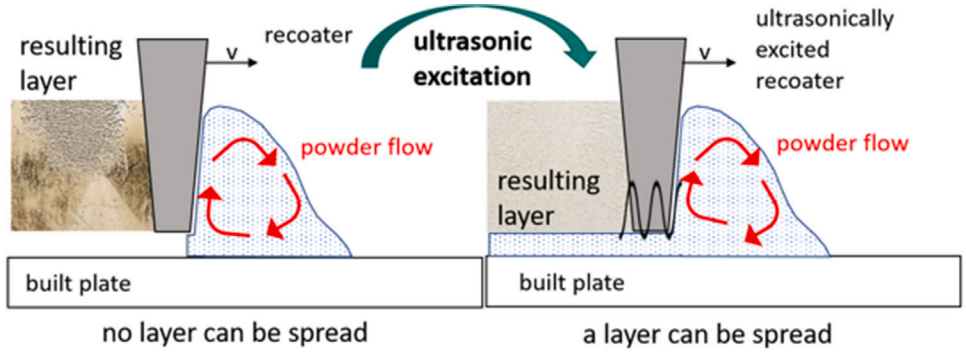

HIGHLIGHTS

- Development of a novel ultrasonically excited recoating system to process agglomerating powder.
- Geometry optimization and definition of a process window for the new recoating system.
- Investigation of the segregation long the recoated length.
- Measurement of the powder layer density for various recoater systems.

ARTICLE INFO

Keywords:
Laser powder bed fusion
Ultrasonic excitation
Powder spreadability
Recoating defects
Recoating process
Agglomerating powder

ABSTRACT

Part quality in laser powder bed fusion is influenced by the uniformity and density of the powder layer. As a result, requirements for the powder regarding spreadability and flowability are restrictive. Many researchers reported recoating defects for cohesive and agglomerating powders. However, the processing of such powders is highly desirable since e.g. surface roughness can be reduced. Therefore, we propose a novel ultrasonically excited recoater system to process such powder. In order to qualify the new recoater system, five different geometries with various amplitudes and recoating velocities were evaluated and compared to a conventional system. The defect rate, determined with a camera and AI-based analysis, the deposited mass and segregation along the recoated distance and the powder layer density of the resulting powder bed were analyzed. A process window and optimal geometry could be identified. It was possible to reduce segregation to a minimum, while maintaining a smooth, dense layer.

* Corresponding author.
E-mail addresses: kai.drechsel@kit.edu (K. Drechsel), victor.lubkowitz@kit.edu (V. Lubkowitz), Lena-Albrecht96@gmx.de (L. Albrecht), uqitq@student.kit.edu (P. Schäfer), markus.schneider@pp-tech.de (M. Schneider), Volker.Schulze@kit.edu (V. Schulze), Frederik.Zanger@kit.edu (F. Zanger).
https://doi.org/10.1016/j.powtec.2023.119153
Received 20 September 2023; Received in revised form 6 November 2023; Accepted 12 November 2023
Available online 14 November 2023

1. Introduction

Laser powder bed fusion of metals (PBF-LB\M) allows near net shape manufacturing of complex geometries. Powder bed based additive manufacturing processes typically consist of three steps [1]. First, the powder feedstock is spread in a thin layer, which is called recoating step. Second, the powder is partially or fully melted by a heat source to create the cross section of the part in the current layer. Third, the built platform is lowered by one layer thickness, typically between 30 µm and 50 µm. The steps are repeated to form a part layer by layer. Powder properties significantly influence process stability and part quality in the first and second step of PBF-LB\M [2]. The most influential properties are particle size distribution (PSD), particle shape, chemical composition and flowability [3]. While the first three properties do not influence each other, powder flowability, as a state, is heavily influenced by all of them [3].

Up to now, many research has investigated the influence of the PSD and particle shape on the PBF-LB\M process and resulting part quality. A negative influence of coarse particles on the part density and the quality of the powder bed was found for 316L [4]. However, fine powders reduced recoatability due to agglomerates [2,5]. Investigations of [5] verified the influence of 316L powder with different PSDs. Coarser particles lead to lower density due to increased spatter, while fine powders with a $d_{50} = 10\,\mu m$, d_{10}, d_{50} and d_{90} representing the particle diameters at 10%, 50%, and 90% in cumulative distribution, did not exhibit sufficient flowability to be recoated. The powder could not be spread in a smooth, even layer, instead agglomerates carved deep and wide grooves into the powder bed. The powder layer formation and melting was simulated by [6]. Finer powder creates a more even powder bed which is important to avoid defects in finished parts, since they stabilize the meltpool. However, particles with a diameter smaller than 10 µm tend to form unwanted agglomerates. The influence of the PSD was also investigated for IN625 powder by [7]. The finest powder investigated, with a d_{90} of 10 µm, could not be processed due to agglomeration. The as-built surface roughness could be reduced with an increased proportion of fine particles [8]. However, the investigations were limited to processable powders. Seven 316L powders with different PSDs were investigated by [2]. The mean particle size as well as the width of the PSD was varied. A mean particle size above 38 µm did influence the stability of the meltpool negatively. Larger particles tend to increase fluctuation of the meltpool width. In contrast to [2,4,5,9] concluded that coarser powders yield less porosity in the finished part. Recoating issues occurred for fine powders as well [9].

A vibration assisted recoating process of the polymer PA12 was simulated by [10], using the Discrete Element Method. The powder bed porosity could be reduced by up to 13.2% in comparison to a conventional recoater. However, only a spreadable polymer powder was investigated and only simulation studies were carried out.

Despite the research carried out to investigate the relation between the PSD and the resulting part density, there still is a gap in knowledge present. Up to now, the processing of fine powders remains challenging. A sufficient flowability is required in order to spread the powder in thin layers during PBF-LB\M. It is difficult to carry out detailed investigation of the relation between layer and part quality and the influence of fine powders due to heterogeneous layers and agglomerates that form during the processing of fine particles. To the best knowledge of the authors all researches were limited to sufficiently well flowing metal powders or recoating defects and inhomogeneities influenced the results.

In this study, a novel recoating process using ultrasonic excitation is proposed to enable the processability of agglomerating and poor flowing powders. First, the used powders are described. Second, the principal of the new recoating system is described in detail. Since the recoating system has never been used before, a comprehensive study on the influence of the recoater geometry, the recoating speed and the amplitude of the recoater is carried out. Achievable quality of the powder bed, the potential effect on segregation along the recoating direction and a process window are not yet known and will be investigated. Therefore, two different 316L powders are compared. One processable with a standard rubber lip recoater, representing the industry standard and one forming severe agglomerates due to a wider PSD including finer particles. For fines particles below 20 µm, Van-der-Waals forces become relevant in relation to the gravitational forces [11,12]. The first will be referred to as powder A. The second is representing a resource efficient powder since none of the around 25% fine particles smaller 20 µm produced in the atomization process were removed. This powder will be referred to as powder B.

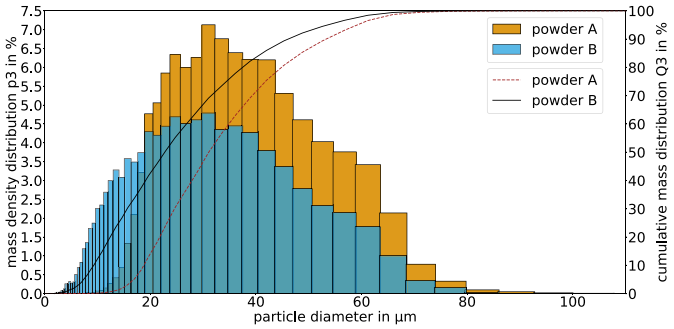

Fig. 1. Particle size distribution of powder A and of powder B plotted as cumulative mass distribution Q3 and the mass density distribution p3.

2. Material and methods

2.1. Powder properties

In order to produce the powder, three batches of 316L were atomized with a Gas-Atomiser AUG 13 000 from BLUEPOWER CASTING SYSTEMS. The three batches of raw powder were mixed and sieved with a mesh size of 63 µm to remove the particles too large to be processed. The powder was then the split into two batches. The first was used in the state with only the particles larger than 63 µm removed. Due to the presence of fine particles Van-der-Waals forces were relevant in comparison to the gravitational force [11,12]. Therefore, powder B was strongly cohesive and agglomerates heavily. For the second batch, particles with a diameter smaller than 20 µm were removed with an Air Classifier AC 1000 G from BLUEPOWER CASTING SYSTEMS. The chemical composition was measured for powder A by the BDG-Service GmbH and is shown in 1. Only the oxygen content was measured for both powders since the specific surface is larger for fine particles, present in powder B, and oxides tend to form on the surface of particles during the cooling [13].

The PSDs of both powders were measured with a Camsizer X2 (Retsch Technology GmbH) using a dispersion pressure of 20 kPa to separate agglomerates into individual particles. The Camsizer uses two cameras, one with a small magnification to capture a sufficient numbers of large particles and one with a large magnification to resolve the small pictures. To quantify the size of particles, the measurement x_{area} was used. x_{area} describes the diameter of a circle with the same area as the area of the analyzed particle and correlates well with the results of the air classifier. However, the mesh size of the sieve correlates better with the minimum length of a particle. The cumulative mass distribution Q3 and the mass density distribution p3 can be seen in Fig. 1.

The span $S = (d_{90} - d_{10})/d_{50}$ represents the width of the Gaussian distribution [14]. The d_{10}, d_{50}, d_{90} and span values are shown in Table 2.

Powder B had a larger span due to the particles smaller 20 µm and the same mesh size used to remove particles larger than 63 µm. The d_{10} of powder A matched the aim of 20 µm, since x_{area} is used to measure the particle diameter. The d_{90} was 4 µm smaller than the mesh size.

Table 1
Chemical composition of the powders in %. Only the Oxygen content was measured for both powders separately.

Alloy	Fe	C	Cr	Ni	Mo	Mn	Si	N	O
Required	Bal.	≤0.03	16.5–18.5	10.0–13.0	2.0–2.5	≤2.0	≤2.0	≤0.1	–
Powder A	68.6	0.017	16.8	10.6	2.12	1.52	0.32	0.031	0.034
Powder B	68.6	0.017	16.8	10.6	2.12	1.52	0.32	0.031	0.048

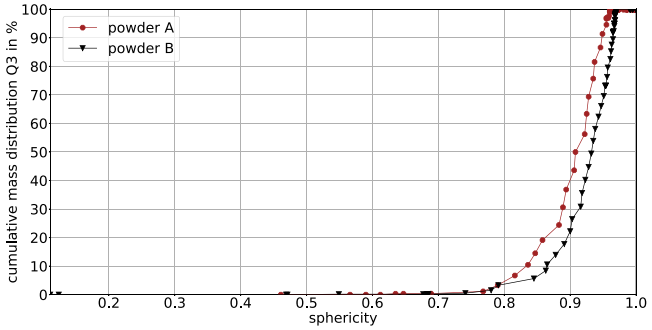

Fig. 2. Comparison of the Q3 over the sphericity of powder A and powder B.

Table 2
Particle size distribution and span of both powders.

Powder	d_{10}	d_{50}	d_{90}	S
A	20.25 µm	33.55 µm	57.52 µm	1.111
B	9.96 µm	24.46 µm	49.62 µm	1.622

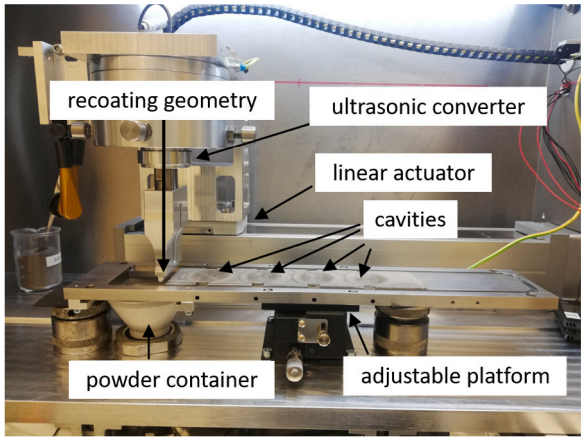

Fig. 3. Adjustable test rig to investigate the recoating process with different recoater systems and experimental setups.

The sphericity is calculated by $SPHT3 = 2\sqrt{\pi A}/P_{real}$, where A is the area and P_{real} is the circumference of the particle. Both powders consisted of mostly spherical particles as it can be seen in Fig. 2. However, powder A was slightly less spherical than powder B.

The apparent and tap density were measured three times according to ASTM B329-20 [15] and ASTM B527-22 [16] for both powders. The Hausner Ratio was calculated as the ratio of tap to apparent density [17]. The results will be presented in Section 2.2.4.

2.2. Recoating process

To investigate the recoating process an adjustable test rig, shown in Fig. 3 was developed. The test rig consists of a spindle screw drive (ELGC-BS-KF-80-300-16P, Festo) with a stroke of 300 mm to drive the recoater. A flexible interface, adjustable in two axes to align the recoater to the build plate, was designed to mount different recoating systems. The usable area of the build plate itself was 50 mm wide with grooves around to catch excess powder. It was mounted on a microscope table to manually adjust the layer thickness with a precision of 5 µm. The build plate can easily be changed depending on the experiment. Glass windows on the top and front allowed an optical observation of the recoating process. To recreate the recoating system in a PBF-LB\M machine, the rubber lip used in an SLM280HL (Nikon SLM Solutions AG) was cut to a length of 50 mm and mounted with the same principle as in the SLM280HL, as it can be seen in Fig. 4(c).

2.2.1. Ultrasonically excited recoating

The novel recoater process utilizes an ultrasonic excitation of the recoater in order to overcome interparticular forces, like friction forces, adhesion due to moisture [18], electrostatic forces [19], magnetic forces [20] and Van-der-Waals forces [11,12]. Especially Van-der-Waals forces become relevant for fine powders [11,12,21]. The effect of ultrasonic vibrations on overcoming and reducing interparticular forces and increasing the flowability of a powder has been shown by [22]. However, it has never been transferred to the recoating in PBF-LB\M.

The recoating geometry in contact with the powder, called sonotrode, was designed to vibrate in resonance at 35 kHz. However, the resonance frequency of the manufactured sonotrodes differed slightly with around 200 Hz below 35 kHz, which is within the control range of the generator. The aluminum alloy EN AW-7075 T6 was used as a material to manufacture the sonotrode. The maximum amplitude was at the tip of the sonotrode. The sonotrode vibrates in a pure transversal motion at the tip, all bending and other eigenmodes were not excited due to the geometrical design. The amplitude can be set freely to a fixed value by the controller, the range is shown in Table 3. During the recoating step, the sonotrode vibrates and transfers energy into the powder. The hypothesis is to break agglomerates apart and overcome interparticular forces of strongly cohesive powders, temporally creating sufficient flowability to spread the powder in a thin layer.

2.2.2. Optical analysis of powder bed quality

In order to analyze the powder bed optically, various powder layers were deposited on the test rig with the parameter settings listed in Table 3. A flat build plate was used for the experiments.

A rubber lip and two sonotrodes were tested while each of the two sonotrodes, named metal flat and metal sharp, had a different geometry feature on each side. Therefore, in total five different recoating geometries were compared. The recoaters are shown in detail in Fig. 4. Both, powder A and powder B were processed with all five geometries.

For the rubber lip, acting as the reference system, no ultrasonic excitation was possible, so only the velocity was varied. However, for the sonotrodes the amplitude was varied in six steps between zero and 14.0 µm for the sharp one and 14.4 µm for the flat one respectively. The chosen amplitudes were controlled by the ultrasonic generator. The smallest amplitude tested, was limited by the generator. With the sonotrodes, all possible combinations of amplitude and velocity were investigated.

To spread the layer 7 ml of powder were placed in front of the sonotrode or rubber lip and distributed along the plate with a defined speed. Excess powder was collected in grooves at the side of the build plate as well as in the end of the plate. This ensures an evenly distributed powder layer without lateral powder accumulations.

For the optical analysis of the powder layers deposited, an iDS U3-3890CP Rev.2.2 camera with a Fujifilm HF2518-12M 25 mm lens was installed. The camera was installed centrally on the ceiling of the

Table 3
Parameters and the according values that were investigated.

Blade geometry	Amplitude in µm flat/sharp	Recoating velocity in mm/s	Amount of powder in ml
Metal, flat r = 0.5 mm	0/0	50	2.5
Metal, flat r = 1.5 mm	6.0/5.7	100	4
Metal, sharp 60°	7.8/7.0	150	7
Metal, sharp 45°	9.8/8.3	200	11
Rubber lip	12.0/11.2	250	
	14.0/14.4	300	
		350	
		400	

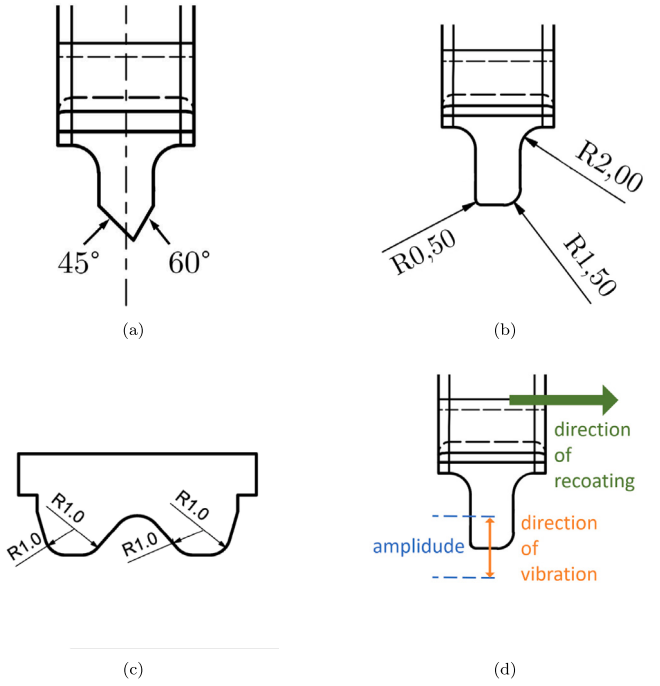

Fig. 4. Geometry of the tip of the sonotrode for (a) the sharp one with a 45° and a 60° edge and (b) the flat geometry with two different radii with 0.5 mm and 1.5 mm radius. (c) Rubber lip from SLM Solutions fixed in the aluminum beam. (d) Visualization of the ultrasonic vibration for both sonotrodes.

test rig and faces down towards the build plate. To illuminate the build plate, four LED strips were mounted on the ceiling of the test rig, which can be controlled individually to achieve the most uniform illumination of the powder layer. The camera delivers greyscale images of 3000 × 4000 pixels. The distance of the camera to the surface of the applied powder layer was 320 mm, resulting in a calculated resolution of the images of 26 µm/pixel.

The software for automated evaluation of the visual quality of the powder layers was implemented in Python utilizing the framework PyTorch. A neural network was used to evaluate the images, similar to [23]. The neural network consists of four convolutional layers, which are suitable for detecting patterns, and five adjoining linear layers. The linear layers summarized the information learned by the convolutional layers to such an extent, that at the end of the neural network there were only two channels. Those channels gave the probability whether an image section is a 'success' or a 'defect'. The image of one layer was divided by a regular grid into small image sections, in order to localize defects in a layer. The individual image sections had a size of 50x50 pixels and overlapped by 50% of their size, i.e. by 25 pixels each. The resulting segmentation is shown in Fig. 5. The overlap ensured that defects located at the edge of an image section and therefore not fully imaged by it were fully covered in the next overlapping image section. With the resolution of 26 µm/pixel, the individual image sections have an edge length of 1.32 mm. The small section were categorized and fed into the neural network. Two categories were defined 'success' and 'defect'. An image section was classified as defect when the powder layer was discontinuous and the build plate underneath was visible or when a dark, rough warp was visible. A powder layer deposited with the rubber lip and powder A was used as a defect free reference powder layer. Therefore, a defect has the minimum size of 1.32 mm by 1.32 mm.

For the training of the neural network, a large number of image sections must be labeled into the categories 'success' and 'defect'. Therefore, a manual labeling of all data is not possible and automatic generated labels are needed [24]. As a first step for the automatic labeling, contiguous areas were manually marked in the original images that are either completely free of defects or heavily affected by defects. All small sections within these contiguous areas were labeled accordingly. To create the training data, layer images of six powder layers were used, from which 63 679 image sections were generated. Of these, 44 159 (69%) of the image sections showed defect-free powder layer areas and 19 520 image sections (31%) were defective. From this labeled data set, 90% of the image sections were used for training and validating the neural network, the rest of the image sections (10%, 6321 image sections) were used as test data. The larger data set was further divided into training data, which was used to train the network by means of back propagation, and the validation data, which was used to check and validate the training progress. The neural network was trained over 10 epochs. The threshold for the categorization as defect is set to 0.9 to ensure that detected defects have a confidence level of 90%. At the end of the training, the image sections of the test data were processed and categorized by the neural network. Since the network did not have access to these image sections in any of the training epochs, an objective impression of the quality of the categorization by the network can be gained with this test data. Based on the categorization of the test data the neural network achieved a F1-score of 91.1%. Based on this score, it was decided that the neural network was capable of automatically analyzing the quality of the powder layers, in order to qualify the novel recoating approach. The proportion of image sections marked as defective was used as a measurement of the quality of a powder layer.

2.2.3. Measuring of deposited mass and segregation

After the optical evaluation of the deposited powder layers, only the best sonotrode geometry was considered further to process powder B. The velocity range was reduced as well to suitable speeds for the subsequent investigations. Therefore, the parameter variations were reduced to the sharp metal blade with amplitudes of 5.7 µm, 8.4 µm and 11.2 µm, the rubber lip and recoating speeds of 50 mm/s, 150 mm/s and 250 mm/s for the investigation of the powder mass and segregation. The deposited mass as well as the particle segregation was measured by using a build plate with four removable cavities, named C1 to C4 to extract samples from the powder bed. The cavities were placed within the build plate along the recoating direction, as shown in Fig. 3. The cavities were filled with powder in ascending order, with C1 being the first and C4 the last to be filled with powder. The center of the cavities were located at 64.5 mm, 112.0 mm, 159.5 mm, 207.0 mm along the recoating direction, with 0 mm as the position of powder deposition.

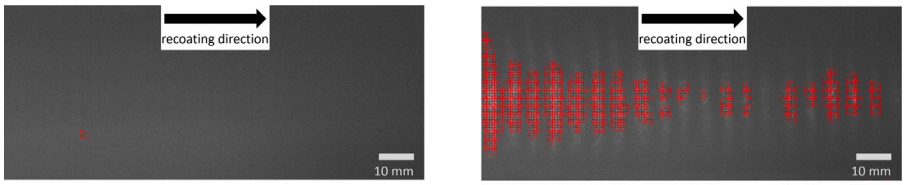

(a) (b)

Fig. 5. Powder layer of powder A recoated with the rubber lip at (a) 100 mm/s recoating velocity and (b) 250 mm/s recoating velocity, with defects marked in red. Each red square correlates to one segment.

The cavities and the build plate were milled from 316L. Their depth was 100 µm and the inner diameter 35 mm. The cavities' rims protrude 100 µm above the build plate. The plate was adjusted accordingly to ensure that the recoating blade's tip just touches the rim of the cavity when spreading the powder to prevent overfilling. However, due to manufacturing tolerances it was not possible to get the recoater to just touch the rims of all geometries. Therefore a gap of 10 µm was used for this experiment.

In order to fill the cavities with powder, changing amounts of powder, as defined in the last column of Table 3 were placed in front of the recoating blade and spread along the platform by the rubber lip or sonotrodes with a specific ultrasonic amplitude and recoating velocity. Each experiment was repeated five times. After the recoating process, the cavities were removed with the help of tweezers and weighted on a high precision scale (Mettler Toledo, XSR204DR) with a precision of 0.1 mg. Additionally, the PSD of the powder inside each cavity was analyzed for every recoater setting. However, the powder in each cavity of the five repetitions were mixed together, in order to have enough particles for a good measurement. A Camsizer X2 with the same setting as described in 2.1 was used to determine the PSD. With this experiment it was possible to investigate segregation phenomena along the recoating direction similar to [25].

2.2.4. Powder layer density

To determine the powder layer density (PLD) it was required, that the entire cavity was completely filled with powder but no particles were left on top of the rim. As described in 2.2.3, due to manufacturing tolerances, the rims of all four cavities were not exactly leveled at the same height. Only the first cavity in recoating direction was filled with powder in order to determine the powder layer density, to make sure the recoater just touches the rim of the cavity. Thereby, the blade is initially placed on the rim of the first cavity and powder was placed in front of the blade, to ensure the cavity is filled only up to the height of the rim. After recoating the cavity with powder, the cavity is removed and weighted on the named precision scale.

To determine the exact volume of the cavity, the real dimensions are used for a calculation, what results in a volume of 97.820 mm^3. After subtracting the tare weight of 65.7148 g of the cavity from the measured weight, the density was determined from the net weight of the powder contained in the cavity divided by the volume of the cavity. Based on the previous experimental results, the variation was reduced even further. Only recoating velocities of 150 mm/s and 250 mm/s were tested for the sharp 60° geometry and the rubber lip. Powder B was processed with 5.7 µm and 8.4 µm amplitude. Powder A was processed with the rubber lip and the sonotrode with no ultrasonic excitation, in order to directly compare the quality of the recoating geometries.

3. Results

3.1. Optical analysis of the powder layers

The results of the optical analysis of powder A show a clear dependency of the powder layer quality on recoating velocity and recoater geometry. Fig. 6 displays the percentage of image sections marked as defects by the image recognition software as a function of the recoating speed. The layers were recoated without ultrasonic excitement. The detected defects represent e.g. heterogeneous layer thicknesses, agglomeration of particles, or other irregularities in the powder layer. A clear trend of an increasing number of defects with increasing recoating speed can be observed for all recoating geometries. The fact that the curves for the flat geometry with r = 1.5 mm and r = 0.5 mm drop between 350 mm/s and 400 mm/s is attributed to an inaccuracy of the image recognition.

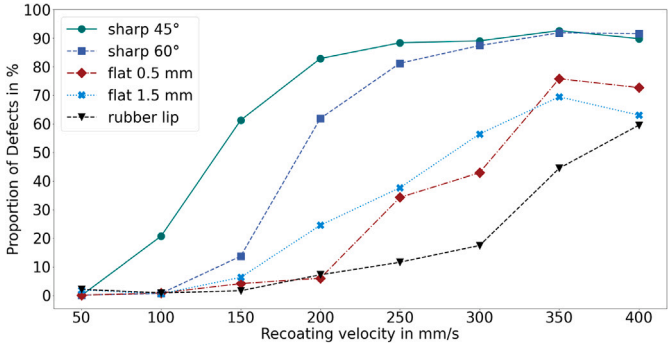

Fig. 6. Defect proportion for powder A with all five recoating geometries.

The rubber lip exhibits the lowest number of defects of all tested geometries. Up to 150 mm/s, the number of defect remains almost constant at a low level. For larger recoating velocities, the quality of the layer decreases, forming irregularities perpendicular to the recoating direction, as it can be seen in Fig. 5(b).

For a velocity up to 150 mm/s, layers recoated with the two flat geometries exhibit a low number of defects. For the geometry r = 1.5 mm the number of defects are comparable with the rubber lip up to 100 mm/s. However, the number of defects increases linear above 150 mm/s. Compared to the geometry r = 0.5 mm, the number of defects start to increase faster and at lower speeds. The geometry r = 0.5 mm exhibits an identical performance than the rubber lip up to 200 mm/s. For higher velocities, the number of defects also increases. Both flat geometries, reaching a maximum number of defects of about 60%–70%.

The sharp 60° geometry exhibits a similar performance as the rubber lip and flat sonotrode up to 100 mm/s. For faster velocities the number of defects increases fast, creating blank stripes in the powder layer perpendicular to the recoating direction, similar to the ones observed with the rubber lip. With the sharp 45° geometry a low number of defects is only achievable with 50 mm/s. The curve of the sharp 45° geometry looks similar to the curve sharp 60° geometry, but the number of defects already start to increase at lower velocities. For a velocity above 250 mm/s, the proportion of defects stagnate at around 90%.

With the rubber lip, the two flat geometries and the sharp 60° geometry, excellent layers with a defect proportion below 2.5% can be generated with a recoating velocity of 100 mm/s.

All five recoating geometries perform very poor when powder layers with powder B without ultrasonic excitation layers were deposited.

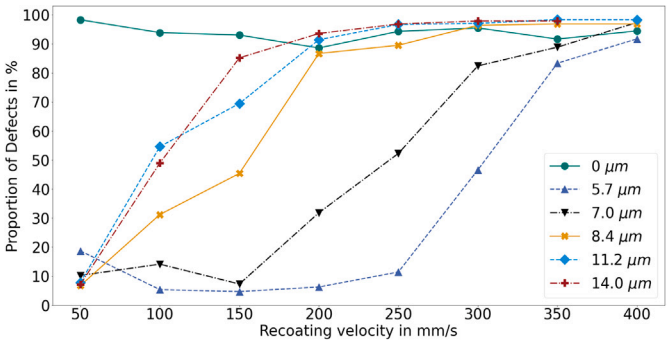

Fig. 7. Defect proportion for powder B with the sharp 45° geometry with amplitudes from 0 µm to 14.0 µm and velocities between 50 mm/s and 400 mm/s.

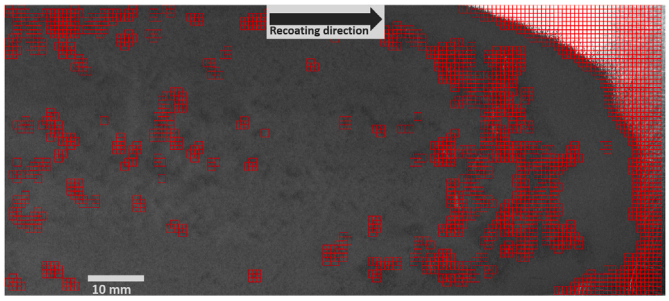

Fig. 8. Powder layer of powder B recoated with sharp 45°, 5.7 µm amplitude and 50 mm/s recoating velocity.

Defect rates exceeded a defect proportion of 84% for all recoating velocities and geometries. The powder layers are found to be highly heterogeneous consisting of mostly blank areas without any powder. With traditional recoating systems, powder B is not processable and therefore unusable for PBF-LB\M.

Thus, the ultrasonically excited powder layers are investigated closely. While the flat geometries outperformed the sharp ones with powder A and no ultrasonic excitation, the attempt to generate useful powder layers with powder B and ultrasonic excitation failed. Even with the smallest possible ultrasound amplitude of 6.0 µm, no powder is deposited to the plate for all velocities. However, the powder is blown away by the vibrations. Therefore, the tested sonotrode geometries for deeper investigation were reduced to the sharp geometries with 45° and 60° inclination, as the rubber lip cannot be excited in resonance with the ultrasonic generator.

For both geometries, recoating without ultrasonic excitation, labeled as amplitude 0 µm, results in a high defect rate between 90 and 100% for all recoating speeds. For both geometries, the number of defects depends strongly on the recoating speed and the amplitude. For the 45° geometry, all amplitudes larger or equal 8.4 µm amplitude, have the lowest defect rate at 50 mm/s (Fig. 7). However, with such a low recoating velocity, the amount of powder is not sufficient to be spread over the entire build plate, as it can been seen in Fig. 8. This effect is the strongest for the slowest velocity. Since the same amount of powder is used for all deposited layers, the deposited layer must either be denser, thicker or more powder is pushed into the grooves of the build plate. Even for 100 mm/s the amount of powder is barley enough to cover the entire build plate, while there is plenty of excess powder at the end of the build plate for other geometries. For larger recoating velocities, the defect rates for amplitudes above 8.4 µm increase and stagnate at around 90%, similar to the results with powder A.

Comparing the individual amplitudes in Fig. 7, it can be observed that an amplitude of 5.7 µm exhibits the fewest detected defects, with less than 8% for velocities between 100 mm/s and 200 mm/s. Above

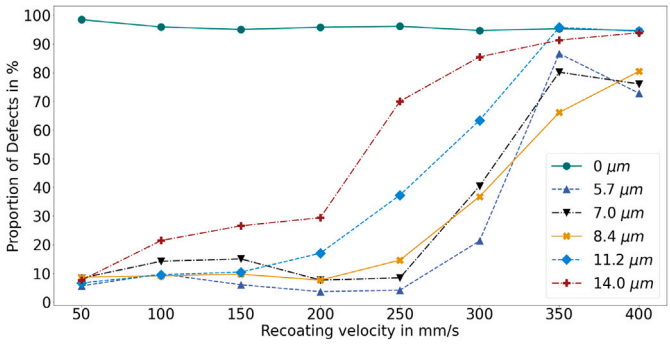

Fig. 9. Defect proportion for powder B with the sharp 60° geometry with amplitudes from 0 µm to 14.0 µm and velocities between 50 mm/s and 400 mm/s.

250 mm/s the defect proportion increases linearly for an amplitude of 5.7 µm. An amplitude of 7.0 µm yields the second-best result, reaching a minimum in defect rate at 150 mm/s. For larger velocities the defect rate increases linearly as well.

For the 60° geometry, all non-zero amplitudes have a similar and low defect proportion for 50 mm/s (Fig. 9). For velocities above 200 mm/s, the defect rate with an amplitude of 11.2 µm and 14.0 µm increase quickly, with the largest amplitude resulting in the highest defect proportion.

For amplitudes up to 8.4 µm the defect rate increases, decreases and increases again between 50 mm/s and 250 mm/s. A minimum in the defect proportion can be observed between 200 mm/s and 250 mm/s. In comparison, the 5.7 µm amplitude exhibits the lowest defect proportion, similar to the results with the 45° geometry.

Comparing both sharp geometries, the data clearly shows a higher sensitivity on the amplitude for the 45° geometry. Especially for velocities below 200 mm/s, the influence of the amplitude on the defect proportion is less for the 60° geometry. As it can be seen in Fig. 7 for the 45° geometry at 200 mm/s, a small increase in the amplitude leads to a drastic increase of defects, while the defect proportion for the 60° geometry (Fig. 9) changes only a bit for amplitudes between 5.7 µm and 8.4 µm This indicates a more stable process window with the sharp 60° geometry for low amplitudes and high recoating velocities.

When comparing the results of ultrasonically excited recoating with powder B with the layers with powder A (Fig. 6), the rubber lip as well as the flat sonotrode geometries still yield in slightly lower defect proportions than the best ultrasonic excited layers. The analysis of the results indicate a shift of the process window to larger velocities for the ultrasonically excited recoating process. However, velocities up to 250 mm/s are not suitable with the rubber lip.

Based on the results presented in Figs. 6 to 9, further recoating experiments with ultrasonic excitation are conducted using both sharp geometries, while the rubber lip will be investigated as reference. However, the focus will be on the 60° geometry since the 45° geometry appears to have a more unstable processing window. The flat geometries will be excluded as they proved to be unsuitable to deposit powder layers with excitation. Additionally, the number of examined amplitudes will be reduced for the further investigations, since the measurement results for the 60° geometry are very close to each other and large amplitudes have a negative influence on the number of defects.

3.2. Deposited mass

In Fig. 10 the deposited mass in each cavity is plotted over the recoated length. The measurement points correspond to the center of the cavities. The velocity varies between 50 mm/s, 150 mm/s, and 250 mm/s for the sharp 60° geometry, with an amplitude of 5.7 µm and a powder mass of 7 ml, shown as the red, blue, and black curves respectively.

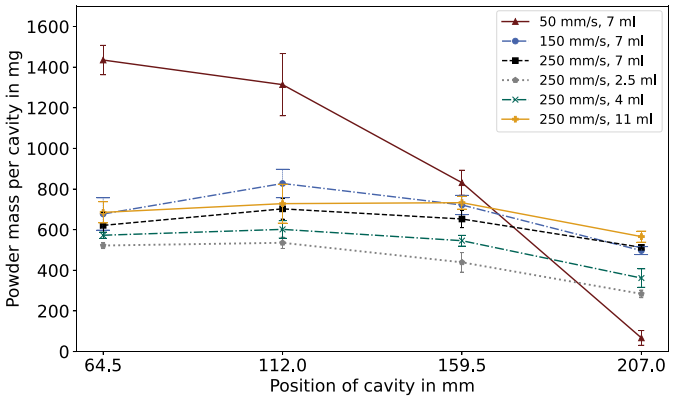

Fig. 10. Deposited powder mass in mg in each cavity for various recoating speeds and amounts of powder used with powder B and the 60° geometry at an amplitude of 5.7 µm.

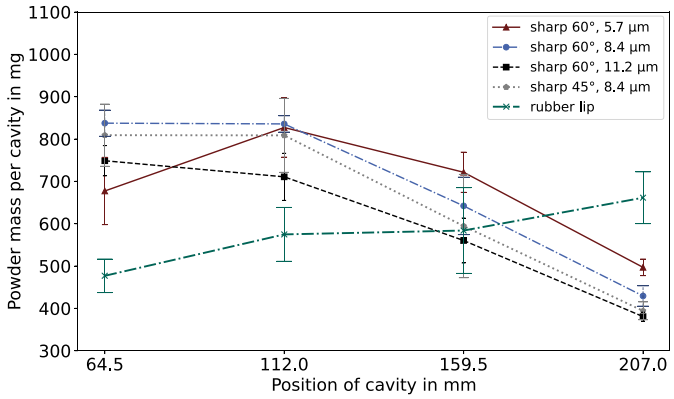

Fig. 11. Deposited powder mass in mg in each cavity with various ultrasound amplitudes and the rubber lip at 250 mm/s for 7 ml powder. Powder A was used for the rubber lip, while powder B was used for the rest.

Additionally, a variation of the deposited powder amounts at a speed of 250 mm/s, with powder masses of 2.5 ml, 4 ml, and 11 ml is represented by the gray, yellow, and green curves. For a slow velocity of 50 mm/s, it is noticeable that a significant amount of powder is deposited in cavity 1 and 2. The thickness of the deposited layer in those cavities must be larger than the 100 µm depth of the cavity plus the 10 µm gap, since the PLD would have to be larger than the material density, if such a weight would be deposited in that volume. The amount of powder drastically decreases for cavity 3 and 4. In the last cavity the amount of powder is nearly zero. With this velocity the amount of powder is not enough to completely fill the last cavity explaining the low amount of powder. Similar effects are described in 3.1 for the sharp 45° geometry at low velocities.

For a speed of 150 mm/s and 250 mm/s, the maximum amount of powder is mostly deposited in the second cavity, except for a velocity of 250 mm/s and a powder amount of 11 ml. In this case the maximum is in the third cavity, but with only minor variation for the first three cavities. Generally, the amount of powder deposited becomes more constant along the recoated distance as the recoating velocity and the used powder volume increases. With an increasing recoating velocity, the powder amount decreases in all cavities. In contrast, with an increasing powder volume, the amount of powder increases in all cavities. The most consistent mass distribution along the recoated length is achieved at a recoating velocity of 250 mm/s and a powder volume of 11 ml followed by 7 ml.

In Fig. 11, the measured powder quantities are shown for the sharp 60° geometry, at a recoating velocity of 250 mm/s, a powder volume of 7 ml and various amplitudes ranging from 5.7 µm to 11.2 µm. As reference, measurements taken with the sharp 45° geometry with an amplitude of 8.4 µm, and the rubber lip with powder A are displayed. Only for the 60° geometry with an amplitude of 5.7 µm the amount of powder increases between the first and second pots, while the measurements for the 8.4 µm amplitude remain constant, and the measurements for the 11.2 µm amplitude decrease. From the second to the fourth cavity the mass decreases for all experiments with the sonotrodes.

The powder mass for the sharp 45° geometry with an amplitude of 8.4 µm is about 3% lower for all cavities compared to the 60° geometry with 8.4 µm amplitude. However, the standard deviation overlap, so there is no significant difference. In general, a larger amplitude reduces the amount of powder deposited in each cavity. Also, the amount of powder in the cavities reduces along the recoating direction. This indicates an velocity and amplitude depending mass deposition due to the ultrasonic excitation. However, the opposite phenomena is observable for the rubber lip with powder A. In contrast to the powder deposition with the vibrating sonotrodes, the deposited mass increases along the recoated length. In the first two cavities, the amount of powder is significantly lower for the rubber lip compared to the two sharp geometries, while the fourth is filled with the most powder.

3.3. Powder layer density

To further advance the assessment of the powder layer quality, the measured PLD is presented in Fig. 12. For comparison, the apparent and tab density are presented as well. The apparent density of powder B is 6.0% larger than for powder A. For the tap density the difference is even smaller with only 4.4%, resulting a slightly larger Hausner ratio of 1.2 for powder A compared to 1.19 for powder B.

For 150 mm/s the PLD for the rubber lip is only 0.1 g lower than the apparent density and 0.91 g above the 60° geometry without ultrasonic excitation. For 250 mm/s the PLD decreases as expected, since the recoating defects were present at this velocity. When comparing the rubber lip and sharp 60° geometry for both velocities, the data clearly shows a larger PLD for the rubber lip. This confirms the results of the optical analysis, where the rubber lip resulted in a lower defect rate. For the 5.7 µm amplitude, a reduction in PLD with increasing recoater velocity can be observed for both powders as well. The PLD of powder A was increased with an amplitude of 5.7 µm, compared to the recoating without excitation. A direct comparison between powder A and B, recoated with the sharp 60° geometry, showed a larger PLD for powder B at 150 mm/s. The PLD of powder B is even larger than the PLD with the rubber lip. For 250 mm/s the PLD of powder A and B is almost identical. For the 8.4 µm amplitude the influence of the velocity is much smaller, resulting in an almost identical PLD for both tested velocities and powders.

3.4. Segregation

A normalized particle diameter is chosen in order to be able to compare the PSD of powder A and B in the cavity. The normalized diameter represents the ratio of the measured diameters in each cavity to the diameters of the entire powder batch. Therefore, a normalized diameter smaller than 1.0 indicates that the particles deposited in the respective cavity are, on average, smaller than the particles in the original powder batch and vice versa. Fig. 13 shows the normalized d_{50} value of powder A recoated with the rubber lip and powder B recoated with the sharp geometries with amplitudes ranging from 5.7 µm to 11.2 µm, all at a speed of 150 mm/s and with 7 ml powder.

All measured values of the normalized d_{50} are greater than 1.0 for the first three cavities. Furthermore, a decreasing d_{50} value along the recoated length can be observed for all but the sharp 60° geometry with an amplitude of 8.4 µm. For the sharp 60° geometry, the largest amplitude results in the steepest gradient along the recoated length. The 8.4 µm amplitude results in the most even distribution. With the smallest amplitude the gradient increases again.

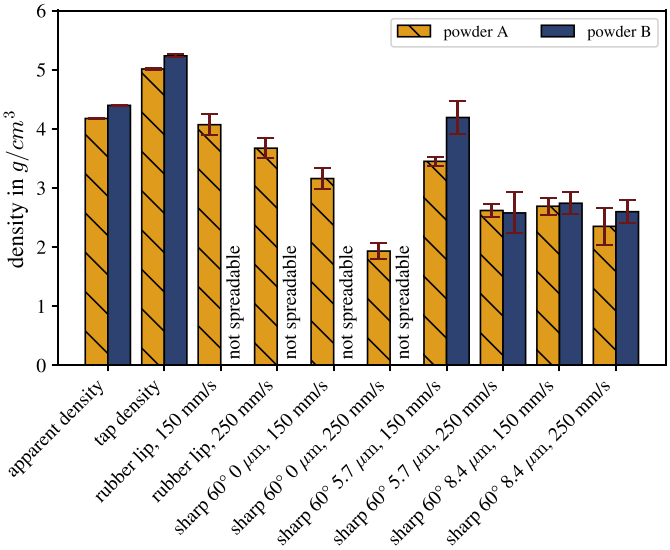

Fig. 12. Apparent, tap and powder layer density for powder A and B. The powder layer density is measured for various recoating geometries, velocities and amplitudes at 20 mm recoated length.

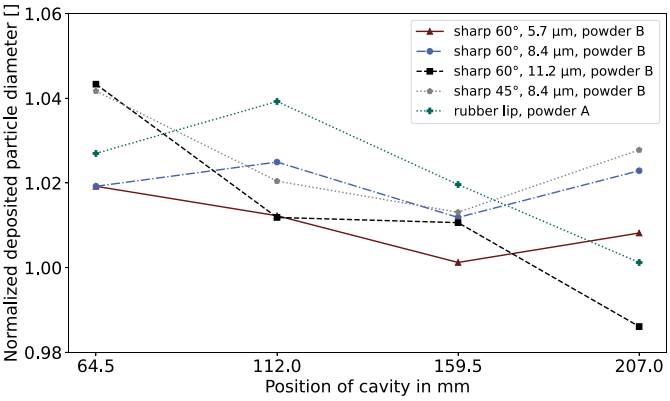

Fig. 13. Normalized d_{50} value in each cavity for a recoating speed of 150 mm/s with the rubber lip, the sharp 45° metal blade and the sharp 60° metal blade with ultrasound amplitudes between 5.7 µm and 11.2 µm.

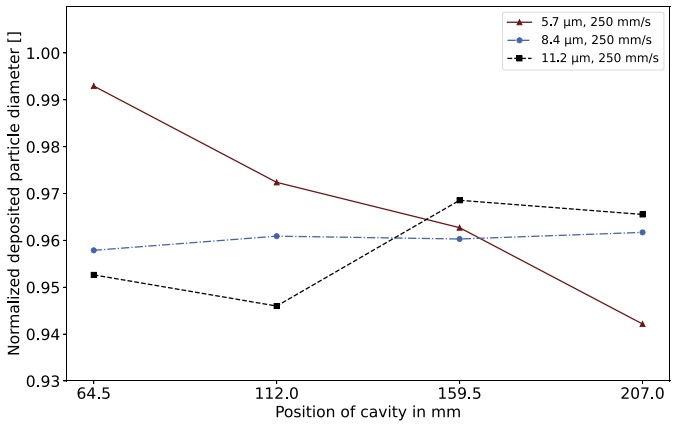

Fig. 14. Normalized d_{90} value for three different amplitudes between 5.7 µm and11.2 µm recoated with a sharp 60° geometry at 250 mm/s and with 7 ml of deposited powder for powder B.

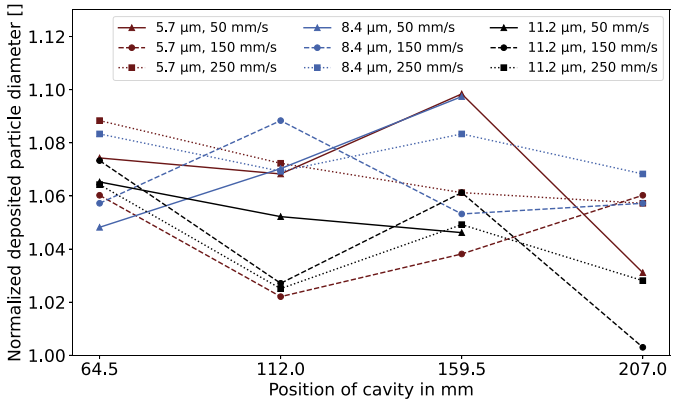

Fig. 15. Normalized d_{10} value along the recoating distance for the sharp 60° geometry with various ultrasound amplitudes and recoating velocities between 50 mm/s and 250 mm/s for powder B.

Except for the first cavity, the sharp 45° geometry with an amplitude of 8.4 µm results in the almost identical normalized d_{50} values compared to the 60° geometry at 8.4 µm. With the rubber lip, the d_{50} value increases during the first 112 mm and reduces with a similar gradient than the sharp 60° geometry with an amplitude of 11.2 µm. Overall, a deposition of coarser particles can be observed. Similar results are obtained for the d_{10} values with the same setting as in Fig. 13. The results of the d_{10} values can be seen in the Appendix in Fig. A.18.

For the rubber lip, the sharp 60° geometry with 11.2 µm amplitude and the sharp 45° geometry, the d_{10} decreases from cavity one to four from 1.07 to 1.03, from 1.08 to 1.0 and from 1.07 to 1.03 respectively. With the sharp 60° geometry with 8.4 µm amplitude, the d_{10} is the most constant. With 8.4 µm amplitude the d_{10} decreases from 1.06 at 64.5 mm to 1.03 at 112.0 mm and increases linear to 1.06 at 207.0 mm. The d_{90} are almost constant and below 1.0 except for the sharp 60° geometry with 8.4 µm amplitude, which results in a d_{90} of 0.96 for cavity one and increases to values between 1.01 and 1.02 for the rest of the recoated length.

For further assessments, the influence of the amplitude on the normalized particle diameter d_{90} is analyzed for the sharp 60° geometry with a larger velocity of 250 mm/s. In contrast to the normalized d_{50} particle diameter, which predominantly yields values greater than one for recoating velocities ranging from 50 mm/s to 250 mm/s, the normalized d_{90} particle diameter for the same velocities mostly exhibits values smaller than one. Fig. 14 illustrates the particle diameter d_{90} dependency on ultrasonic amplitudes ranging from 5.7 µm to 11.2 µm for 250 mm/s. With an amplitude of 8.4 µm the d_{90} remains nearly constant and below 1.0 across the four cavities (Fig. 14), while for 150 mm/s the $d90$ is greater than 1.0 (Fig. A.19). In contrast, the d_{90} for the powder layer with a 5.7 µm amplitude continuously decreases over the recoated length. The particle diameter decreases from d_{90} = 49.27 µm at 64.5 mm to a d_{90} = 46.75 µm at 207 mm, which corresponds to a reduction of approximately 5%. From the beginning to the end of a layer recoated with an amplitude of 11.2 µm, the d_{90} increases slightly. However, the trend is not monotone.

An increase in the d_{50} value and a decrease in the d_{90} implies a more narrow PSD. Since the difference between powder A and B is mainly in the amount of fines, the results of the measured d_{10} values are presented in detail in Fig. 15. All measurement results show a normalized d_{10} greater than 1.0 with a change of up to 10%. A 10% change corresponds to a 1 µm increase of the d_{10}. For layers recoated with the lowest velocity of 50 mm/s and amplitudes of 8.3 µm and 11.2 µm, the measurement results for the fourth cavity are missing because the powder is fully deposited after reaching the third cavity, as it is described in 3.1 and Fig. 8 already. For the 5.7 µm amplitude, all four cavities could be filled with powder for 50 mm/s, which was not possible with the other two amplitudes.

For the 8.4 µm and 11.2 µm amplitude, the velocity appears to have little influence on the resulting d_{10} value. However, the deposited

powder gets finer along the recoated length for the 11.2 µm amplitude, while the 8.44 µm amplitude results in the smallest gradient. This result is in accordance to the results obtained for the d_{50}. On average the 8.4 µm amplitude results the largest d_{10} values. For the smallest amplitude, the d_{10} scatters the most for different velocities, with no clear trends observable. Overall, the ultrasonically excited recoating leads to a narrower PSD than the original powder B, with smaller d_{90} and larger d_{10} values.

4. Discussion

4.1. Optical analysis of the powder layers

Spreadability of power is defined as the ability of a powder to flow through a narrow gap and form a flat powder layer and depends on the recoater used as well as the process parameters [26,27]. Therefore, the test rig, the different build plates and the AI algorithm was developed to assess the powder bed quality.

As the data in Fig. 6 shows, the best results for powder A can be achieved with flat recoating geometries such as the rubber lip and the flat sonotrode. [28,29] reported similar relations. At low recoating velocities the flow of the powder through the gap is sufficient to create a homogeneous powder bed without any blank areas. As reported by [30], up to a critical velocity the mass flow increases proportionally with the recoating velocity. Due to this phenomenon, the number of defects remains low, even for higher velocities. The critical velocity is the velocity at which an increase in recoating velocity does not further increase the mass flow. For the rubber lip, the critical velocity appears to be at 150 mm/s, for the flat geometries somewhere in between 100 mm/s and 150 mm/s, given the resolution of the experiments. With the flat 1.5 mm geometry slightly more defects are detected at 150 mm/s than for the flat 0.5 mm geometry (Fig. 6). The lower defect rate indicates that the 0.5 mm is closer to an optimal edge radius, found by [28]. While a sharp edge results in a line contact between powder and recoater, which causes a rougher powder bed as particles get dragged along at the edge [31], a small radius at the edge improves the quality of the powder layer significantly [28]. With an increasing radius, the quality decreases again [28]. This could be due to a compacting of the powder, and therefore jamming of the gap, at the large radius, since it can exert a downward facing force component on the particles. With a smaller radius, the powder might be sheared rather than pressed together. In general the larger contact area of the flat geometries helps to smoothen the surface of the powder bed by pressing particles into the bed, as proposed by [29]. For the dual edges rubber lip, high speed camera videos of the recoating process show an additional pile of powder in front of the second edge, as it can be seen in Fig. 16. An additional smoothing effect is provided by the second lip as well as a powder reservoir to compensate flow irregularities at the first edge, explaining the superior properties of the rubber lip.

For higher recoating velocities, defects tend to appear at the beginning of the recoating process. The second powder pile is not present in the beginning of the recoating processes and therefore cannot compensate any irregularities that occur at higher velocities.

The higher defect rate of the two sharp edged geometries could be a result of the line contact, causing the particles to be dragged long rather than spread in a smooth layer. The flat tilt surface (Fig. 4(a) and (b)) might compress the powder before it reaches the edge. A stronger compression increases the shear strength [32], which could cause the mass flow to become irregular and the number of defects to increase. For the 60° geometry, the critical velocity, defined by [30], appears to be at 100 mm/s, while for the 45° geometry it appears to be at 50 mm/s. This could be due to the larger angle, which causes a larger downwards facing force component on the powder compacting it more and therefore limiting the mass flow through the gap.

The analysis of powder B clearly shows, that none of the tested geometries is able to spread powder B in a thin layer. Since powder B consists of many fine particles below 20 µm, large agglomerates form within the powder. These agglomerates do not break apart with traditional recoaters. However, when applying an ultrasonic excitation, a sufficient amount of energy is transmitted into the powder, likely causing the agglomerates to break apart. While the flat geometries have numerous advantages over the sharp geometries, the opposite result is observed with the ultrasonic excitation. Pressure waves in the air between the build plate and the sonotrode, caused by the vibration, could eject the particles out of the gap, reducing the mass flow to almost zero. Or preventing powder to enter the gap in the first place. As a result, no powder is left on the build plate. This result is in contrast to the compaction achieved in [10] with such a flat geometry. For large frequencies and amplitudes particles enter a vibro-fluidized state and therefore the PLD is reduced [10]. Since the frequency in this study and therefor the transmitted energy is much larger than in [10], the negative effect of the vibro-fluidization with flat geometries his increased further.

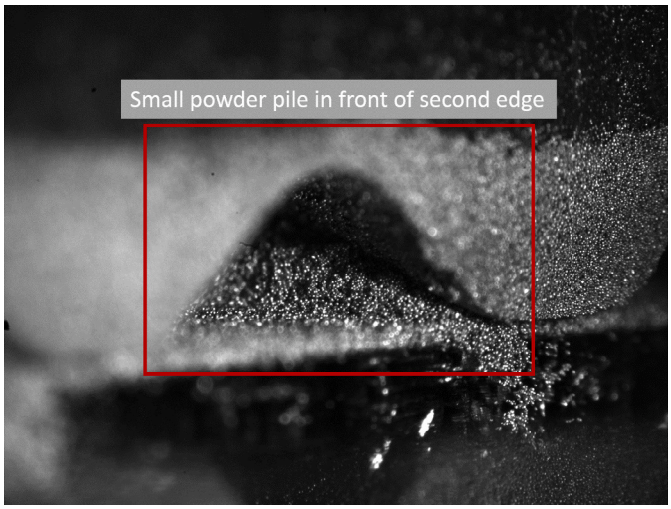

Fig. 16. High speed camera images of the recoating process of powder A with the rubber lip at 50 mm/s.

However, the sharp geometries do not have such a long narrow gap and therefore the powder particles can flow through the gap. When comparing the sharp 45° (Fig. 7) and 60° (Fig. 9) geometry, the data shows a larger influence of the amplitude for the 45° angle. As mentioned earlier, the downward facing force component is larger for this geometry. This could result in pressure waves pushing the powder away from the sonotrode similar to the flat geometries, limiting the mass flow through the gap. For the 60° angle, the movement of the sonotrode causes less of a stamping effect pushing the powder away. Therefore, the mass flow is less sensitive to a change in amplitude. This theory would also explain, why the powder was not enough to cover the entire build plate as reported in Fig. 8. At low recoating velocities, the powder has more time to be pushed away by the pressure waves, causing it to travel sideways into the grooves around the build plate. Further research, simulating the excited recoating is necessary to investigate this effect in more detail. With even larger amplitudes the pressure waves caused by the larger amplitudes hinder the mass flow though the gap as observed for the 45° geometry.

For the 60° geometry with an amplitude of 8.4 µm and 11.2 µm, the proportion of recoating shows no local minimum. High speed camera videos show a fluidized bed around the sonotrode for an increased amplitude while agglomerates are visible in the powder pile for an amplitude of 5.7 µm, as it can be seen in Fig. 17.

Due to this effect, the results could be more similar to the flat geometries and rubber lip in Fig. 6. The excitation and resulting fluidization could stabilize the mass flow through the gap for a wide range of recoating velocities. The largest amplitude transmits too much energy into the powder and causes blank spaces in the layer.

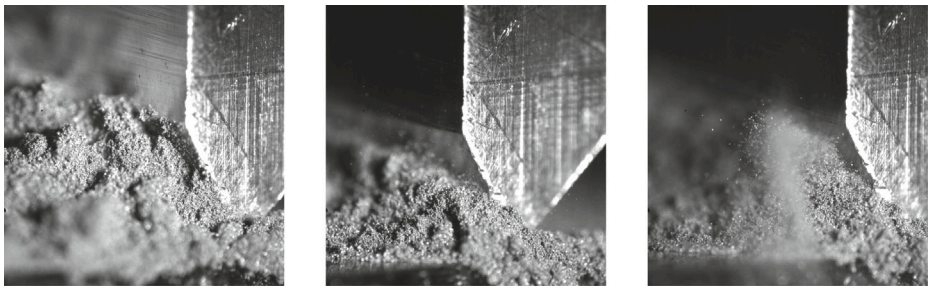

Fig. 17. High speed camera image of the 60° geometry at 150 mm/s with (a) no ultrasonic excitation, (b) an amplitude of 5.7 μm and (c) an amplitude of 8.4 μm.

For the two smallest amplitudes, a local maximum followed by a local minimum in the defect proportion (Fig. 9) is observed. In the velocity range of the local maximum, most defects are detected at the beginning of the recoating process. Since the powder pile is stationary in the beginning and the powder is not fully fluidized at the small amplitudes (Fig. 17(b)), interlocking forces have to be overcome. Once enough energy is transmitted into the powder, it is free flowing [33]. This might explain why the defects are concentrated at the beginning of the recoating process.

In the velocity range of the local minimum, no concentration of defects in the beginning is found. As discussed earlier, the mass flow needs to be constant for a smooth powder layer and with an increasing recoating velocity, the mass flow increases [30]. The data indicates, that for certain recoating velocities the incipient flow happens faster and therefore, the mass flow is more stable from the beginning preventing defects. This could be due to the additional energy provided by the faster translational motion. A larger recoating velocity causes the powder to circulate [34], which could improve the deagglomerating.

4.2. Deposited mass

The deposited mass changes significantly along the recoated length for lowest recoating velocity (Fig. 10). As described earlier, at a low recoating velocity the powder has more time to be pushed away by the pressure wave and can move perpendicular to the recoating direction and out of the way of the recoater. Therefore the pile in front of the sonotrode gets much smaller, yet same energy is transmitted into the powder by the sonotrode. This causes the powder layer to spread thinner. The thinner spread powder layer cannot be detected by the optical analysis as long as it remains homogeneous and optically dense. A faster recoating velocity and a larger amount of powder deposited in front of the sonotrode effectively reduces the gradient in deposited mass along the recoating direction. In this case, even at the last cavity a sufficient amount of powder remains in front of the sonotrode to reduce the thinner spreading due to a smaller amount of powder. For the lowest velocity, the first two cavities are clearly overfilled. A video of the recoating process shows, that powder is spilled onto the cavity in the moment, the sonotrode passes the rim of the cavity. The sudden change in layer thickness after the cavity (they protrude 100 μm) causes the sonotrode to transport an excessive amount of powder through the gap. This phenomena is not present for larger recoating velocities.

At 250 mm/s the rubber lip results in a much lower deposited mass as with the vibrating sonotrodes, since recoating defects start to appear at that velocity. The mass in the cavities is rising along the recoating direction, which [25] reported for steel as well. Since the pile of powder is stationary in the beginning, the incipient flow could explain the lower mass in the first cavity [29]. The same effect could explain the lower mass deposited in the first cavity at the lowest amplitude, since the powder is not fluidized (Fig. 17(b)). At higher amplitudes, the deagglomeration happens faster and therefore a larger mass can be deposited in cavity one, while with the low amplitude the deagglomeration takes more time to fully develop. With an increasing amplitude the overall amount of powder deposited reduces, since the larger amplitude might cause a looser packing density, as [10] predicted in their simulation.

4.3. Powder layer density

The wider span and the finer particles of powder B lead to a higher apparent density, as reported by [27]. The tap density is larger for powder B as well, however the Hausner ratio is slightly smaller than for powder A. This indicates, that the Hausner Ratio does not correlate with spreadability. In contrast to [3], the subjective perception of powder B does not indicate a free flowing behavior, while the Hauser Ratio is in a similar order to his results. The PLD measurements for the rubber lip confirm the theory of a compression of the powder bed when using a recoater with a large surface area, since the PLD is larger than for the 60° geometry. With an increasing velocity, the PLD reduces. This trend was observed in simulation studies by [35] as well. The sharp 60° geometry results in a lower PLD for both tested velocities compared to the rubber lip. The sharp edge causes a rougher and lighter packed powder bed, as reported by [31] as well. The PLD is comparable to the results of [3,36], who also used a sharp blade as a recoater.

With powder B the PLD can be increased compared to powder A, due to the wider span and finer particles [27]. Overall, ultrasonic excitation increased the PLD of both powders and spreadability of a powder can be effectively improved. However, for powder A a flat recoater geometry had a larger positive influence on the PLD than ultrasonic excitation.

The smallest amplitude was limited by the generator, as mentioned in 3.1. Since the defect rate decreased and PLD increased with a smaller amplitude and got worse without ultrasonic excitation, an optimal amplitude should exist. The observed optimum in the experiments was 5.7 μm, respecting the possible amplitudes in the experimental set up. However, with the sonotrodes used it cannot be determined, if even smaller amplitudes lead to an even better layer quality.

An increase in amplitude reduces the PLD. This confirms the hypothesis made in Section 4.2, of a looser packing density for an increased amplitude. The vibro-fluidized state, shown in Fig. 17(c), decreases the PLD and confirms the simulation results of [10]. Interestingly, the recoating velocity appears to have only little influence for larger amplitudes. As discussed earlier, the large amplitude fluidizes the powder around the sonotrode. This easy flowing powder might not be influenced by the recoating velocity so much. The optical analysis is not able to detect differences in PLD, as long as the layer remains dense and smooth. Therefore multiple criteria must be used to evaluate the quality of a powder layer.

4.4. Segregation

The decrease of the d_{50} along the recoated length for all but the 8.4 μm amplitude (Fig. 13) was most likely due to the “brazil-nut

effect", where larger powder particles flow at the bottom of the powder pile [37]. Simulations by [34] confirm this theory. [25] reported a decrease in particle size as well. However the d_{10}, d_{50} and d_{90} were below the values of the entire batch. In this study only the d_{90} is below the d_{90} of the initial powder. Since five layers were deposited for each tested setting, an influence due to the extraction of a small amount of powder is unlikely. The larger d_{10} and d_{50} might be a result of the narrow build plate. Small particles tend to sink to the bottom of the pile in front of the recoater geometry [34]. Since some of the powder was pushed into the grooves on the side, it is possible that more fine particles were pushed away from the sonotrodes and deposited in there.

For the 5.7 µm amplitude, the segregation of large particles is the strongest, while no segregation is observed for the 8.4 µm amplitude, as the d_{90} in Fig. 14 shows. A convective motion in the powder pile can suppress the segregation phenomena [34]. High speed camera videos indicate such a convective motion, however it is not possible to observe the inside of the powder pile. The same applies for the d_{10} values in Fig. 15. The velocity has no influence on the segregation along the recoated direction for the 8.4 µm amplitude. The same independency from the velocity is observed by the other experiments for this amplitude.

With the largest amplitude, more fines were deposited along the recoated length. At the lowest velocity the powder was not enough to fill the last cavity, due to the effects discussed earlier. With an increasing recoating velocity, the powder has less time to be pushed into the grooves at the side of the build plate. The normalized d_{10} of almost 1.00 for the last cavity is another indicator that more fines get pushed into the grooves at the side of the build plate since the fine particles remain in the powder and were not ejected into the environment. Therefore the deposited powder might be slightly coarser than the initial batch in contrast to the results of [25].

5. Conclusion

In this study a novel recoating system was proposed to process severely agglomerating metal powder in PBF-LB\M. A test rig was built to investigate two different powders, one representing processable powders and one representing non-processable powders considering state of the art recoating systems. The optical appearance, the deposits mass and segregation along the recoated length and the powder layer density are analyzed for five different recoater geometries with variating velocities and amplitudes. The following conclusions are reached.

A flat recoating geometry with a small radius was found to be optimal for processing non-agglomerating powders. The results of [28,29,31] were confirmed. Additionally, it is shown that a flat large contact area compresses the powder bed above the apparent density. A dual edged recoater was able to compensate mass flow irregularities, since a second small powder pile is created in front of the second edge.

The approach of utilizing an ultrasonically excited recoater proved to be suitable to process agglomerating powders. In contrast to the traditional recoaters, a sharp edged geometry with an incline angle of 60° was found to be optimal to effectively deagglomerate the powder and still produce a smooth and dense powder layer. A process window was found between a recoating velocity of 150 mm/s and 250 mm/s and an amplitude between 5.7 µm and 8.4 µm. In this range the most even powder layers in terms of roughness, mass distribution and segregation were found. While the powder was the smoothest for an amplitude of 5.7 µm, the other properties were superior at an amplitude of 8.4 µm. Segregation along the recoated length can be suppressed with an amplitude of 8.4 µm.

The recoating velocity depended PLD was larger for powder B than for powder A when comparing the same recoater geometry. An amplitude of 8.4 µm reduced the velocity dependency to a minimum.

The maximum recoating velocity can and should be increased with the use of ultrasonic excitation. A faster recoating velocity effectively reduces the built time in the PBF-LB\M process, since parts consist of up to a few thousand layers.

Further studies are necessary to optimize the recoater geometry since only two different angles were tested. A dual edged design, as used with the rubber lip, can be transferred to a sonotrode and should be investigated in future studies. Additionally, the usability of the proposed recoater system should be tested in a PBF-LB\M process when applying multiple layers. The new recoating systems could enable the processing and investigation of the potentials of non-spreadable powders when melted in a PBF-LB\M machine.

CRediT authorship contribution statement

Kai Drechsel: Conceptualization, Methodology, Validation, Writing – original draft, Formal analysis, Project administration, Supervision. **Victor Lubkowitz:** Conceptualization, Writing – review & editing. **Lena Albrecht:** Investigation, Formal analysis, Validation, Visualization. **Paul Schäfer:** Software, Data curation. **Markus Schneider:** Conceptualization, Investigation. **Volker Schulze:** Resources, Writing – review & editing. **Frederik Zanger:** Funding acquisition, Writing – review & editing.

Declaration of competing interest

The authors declare that they have no known competing financial interests or personal relationships that could have appeared to influence the work reported in this paper.

Data availability

Data will be made available on request.

Acknowledgments

The authors would like to thank Dr.-Ing- Jörg Fischer-Bühner for providing us access to the air classifier and the Camsizer X2 and Daniel Beckers for atomizing the raw powder.

Funding

The presented work was funded by the Ministry of Science, Research and the Arts of the Federal State of Baden-Wuerttemberg within the 'InnovationCampus Future Mobility', which is gratefully acknowledged.

Appendix. Segregation

See Figs. A.18 and A.19.

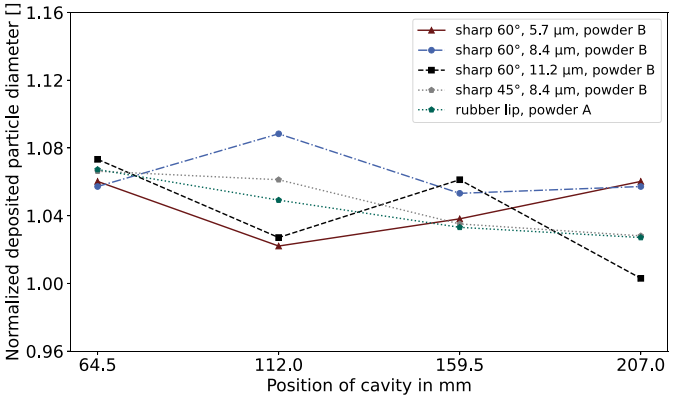

Fig. A.18. Normalized d_{10} value in each cavity for a recoating speed of 150 mm/s with the rubber lip, the sharp 45° metal blade and the sharp 60° metal blade with ultrasound amplitudes between 5.7 µm and 11.2 µm.

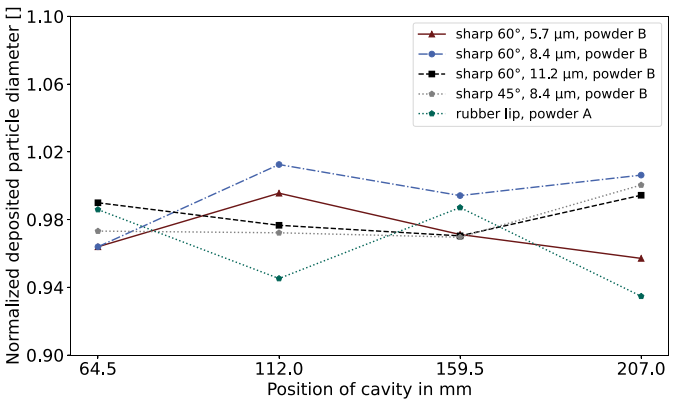

Fig. A.19. Normalized d_{90} value in each cavity for a recoating speed of 150 mm/s with the rubber lip, the sharp 45° metal blade and the sharp 60° metal blade with ultrasound amplitudes between 5.7 µm and 11.2 µm.

References

[1] W. Meiners, Direktes Selektives Laser Sintern Einkomponentiger Metallischer Werkstoffe (Dissertation), 1999.

[2] M.A. Spurek, L. Haferkamp, C. Weiss, A.B. Spierings, J.H. Schleifenbaum, K. Wegener, Influence of the particle size distribution of monomodal 316L powder on its flowability and processability in powder bed fusion, Prog. Addit. Manuf. 7 (4) (2022) 533–542, http://dx.doi.org/10.1007/s40964-021-00240-z.

[3] L. Haferkamp, L. Haudenschild, A. Spierings, K. Wegener, K. Riener, S. Ziegelmeier, G.J. Leichtfried, The influence of particle shape, powder flowability, and powder layer density on part density in laser powder bed fusion, Metals (11) (2021) http://dx.doi.org/10.3390/met11030418.

[4] A.B. Spierings, N. Herres, Levy G., Influence of the particle size distribution on surface quality and mechanical properties in additive manufactured stainless steel parts, Rapid Prototyp. J. (17.3) (2011) 195–202.

[5] S. Ziri, A. Hor, C. Mabru, Combined effect of powder properties and process parameters on the density of 316L stainless steel obtained by laser powder bed fusion, Int. J. Adv. Manuf. Technol. 120 (9–10) (2022) 6187–6204, http://dx.doi.org/10.1007/s00170-022-09160-w.

[6] F.-J. Gürtler, M. Karg, M. Dobler, S. Kohl, I. Tzivilsky, M. Schmidt, Influence of powder distribution on process stability in laser beam melting: Analysis of melt pool dynamics by numerical simulations, in: International Solid Freeform Fabrication Symposium, 2014.

[7] C. Pleass, S. Jothi, Influence of powder characteristics and additive manufacturing process parameters on the microstructure and mechanical behaviour of Inconel 625 fabricated by Selective Laser Melting, Addit. Manuf. 24 (2018) 419–431, http://dx.doi.org/10.1016/j.addma.2018.09.023.

[8] P. Fischmann, F. Schrauth, F. Zanger, Influence of particle size distribution on surface roughness in powder bed fusion - A contribution to increase resource efficiency, CIRP Annals 72 (1) (2023) 145–148, http://dx.doi.org/10.1016/j.cirp.2023.04.018.

[9] M.A. Balbaa, A. Ghasemi, E. Fereiduni, M.A. Elbestawi, S.D. Jadhav, J.-P. Kruth, Role of powder particle size on laser powder bed fusion processability of AlSi10mg alloy, Addit. Manuf. 37 (2021) 101630, http://dx.doi.org/10.1016/j.addma.2020.101630.

[10] D. Schiochet Nasato, H. Briesen, T. Pöschel, Influence of vibrating recoating mechanism for the deposition of powders in additive manufacturing: Discrete element simulations of polyamide 12, Addit. Manuf. 48 (2021) 102248, http://dx.doi.org/10.1016/j.addma.2021.102248.

[11] K. Thalberg, D. Lindholm, A. Axelsson, Comparison of different flowability tests for powders for inhalation, Powder Technol. 146 (146 // 3) (2004) 206–213, http://dx.doi.org/10.1016/j.powtec.2004.08.003.

[12] M. Krantz, H. Zhang, J. Zhu, Characterization of powder flow: Static and dynamic testing, Powder Technol. 194 (3) (2009) 239–245, http://dx.doi.org/10.1016/j.powtec.2009.05.001.

[13] Y. Liu, J. Fang, D. Liu, Z. Lu, F. Liu, S. Chen, C.T. Liu, Formation of oxides particles in ferritic steel by using gas-atomized powder, J. Nucl. Mater. 396 (1) (2010) 86–93, http://dx.doi.org/10.1016/j.jnucmat.2009.10.057.

[14] A.W. Jenike, Storage and Flow of Solids, Bulletin No. 123, Utah State University, 1964, URL https://cir.nii.ac.jp/crid/1571698600138147712.

[15] ASTM, Standard test method for apparent density of metal powders and compounds using the scott volumeter.

[16] ASTM, Standard test method for tap density of metal powders and compounds.

[17] H.H. Hausner, Friction Conditions in a Mass of Metal Powder, Polytechnic Inst. of Brooklyn. Univ. of California, Los Angeles, 1967, URL https://www.osti.gov/biblio/4566075.

[18] E. Emery, J. Oliver, T. Pugsley, J. Sharma, J. Zhou, Flowability of moist pharmaceutical powders, Powder Technol. (189) (2009) 409–415, http://dx.doi.org/10.1016/j.powtec.2008.06.017.

[19] E. Mersch, G. Lumay, F. Boschini, N. Vandewalle, Effect of an electric field on an intermittent granular flow, Phys. Rev. E (81) (2010) URL 10.1103/PhysRevE.81.041309.

[20] A.J. Forsyth, S.R. Hutton, M.J. Rhodes, C.F. Osborne, Effect of applied interparticle force on the static and dynamic angles of repose of spherical granular material, Phys. Rev. E 63 (63 // 3 Pt 1) (2001) 031302, http://dx.doi.org/10.1103/PhysRevE.63.031302.

[21] Y. Ma, T.M. Evans, N. Philips, N. Cunningham, Numerical simulation of the effect of fine fraction on the flowability of powders in additive manufacturing, Powder Technol. (360) (2020) 608–621, http://dx.doi.org/10.1016/j.powtec.2019.10.041.

[22] P. Dunst, P. Bornmann, T. Hemsel, W. Sextro, Vibration-assisted handling of dry fine powders, Actuators (2018) http://dx.doi.org/10.3390/act7020018.

[23] J. Voigt, M. Moeckel, Benchmarking a multi-layer approach and neural network architectures for defect detection in PBF-LB/M, Mater. Today Commun. 33 (2022) 104878, http://dx.doi.org/10.1016/j.mtcomm.2022.104878.

[24] M. Bauer, C. Augenstein, M. Schäfer, O. Theile, Artificial intelligence in laser powder bed fusion procedures – Neural networks for live-detection and forecasting of printing failures, Procedia CIRP 107 (2022) 1367–1372, http://dx.doi.org/10.1016/j.procir.2022.05.159.

[25] G. Jacob, C.U. Brown, A. Donmez, The Influence of Spreading Metal Powders with Different Particle Size Distributions on the Powder Bed Density in Laser-Based Powder Bed Fusion Processes, US Department of Commerce, National Institute of Standards and Technology, Gaithersburg, MD, 2018, http://dx.doi.org/10.6028/NIST.AMS.100-17, (100–17).

[26] M. Ghadiri, M. Pasha, W. Nan, C. Hare, V. Vivacqua, U. Zafar, S. Nezamabadi, A. Lopez, M. Pasha, S. Nadimi, Cohesive powder flow: Trends and challenges in characterisation and analysis, KONA Powder Part. J. 37 (2020) 3–18, http://dx.doi.org/10.14356/kona.2020018.

[27] S. Vock, B. Klöden, A. Kirchner, T. Weißgärber, B. Kieback, Powders for powder bed fusion: a review, Prog. Addit. Manuf. 4 (4) (2019) 383–397, http://dx.doi.org/10.1007/s40964-019-00078-6.

[28] S. Haeri, Optimisation of blade type spreaders for powder bed preparation in Additive Manufacturing using DEM simulations, Powder Technol. 321 (2017) 94–104, http://dx.doi.org/10.1016/j.powtec.2017.08.011.

[29] T.-P. Le, X. Wang, K.P. Davidson, J.E. Fronda, M. Seita, Experimental analysis of powder layer quality as a function of feedstock and recoating strategies, Addit. Manuf. 39 (39) (2021) 101890, http://dx.doi.org/10.1016/j.addma.2021.101890.

[30] W. Nan, M. Ghadiri, Numerical simulation of powder flow during spreading in additive manufacturing, Powder Technol. 342 (2019) 801–807, http://dx.doi.org/10.1016/j.powtec.2018.10.056.

[31] S. Haeri, Y. Wangb, O. Ghitab, Sunc J., Discrete element simulation and experimental study of powder spreading process in additive manufacturing, Powder Technol. (306) (2016) 45–54, http://dx.doi.org/10.1016/j.powtec.2016.11.002.

[32] D. Schulze, Powders and Bulk Solids: Behavior, Characterization, Storage and Flow, second ed., Springer, Cham, 2021.

[33] G. Lumay, N. Vandewalle, C. Bodson, L. Delattre, O. Gerasimov, Linking compaction dynamics to the flow properties of powders, Appl. Phys. Lett. 89 (9) (2006) http://dx.doi.org/10.1063/1.2338801.

[34] A. Phua, C. Doblin, P. Owen, C.H.J. Davies, G.W. Delaney, The effect of recoater geometry and speed on granular convection and size segregation in powder bed fusion, Powder Technology (ISSN: 00325910) 394 (394) (2021) 632–644, http://dx.doi.org/10.1016/j.powtec.2021.08.058.

[35] Y. Lee, S. Simunovic, A.K. Gurnon, Quantification of Powder Spreading Process for Metal Additive Manufacturing (Ph.D. thesis), Oak Ridge, TN, USA, 2019, URL CRADA/NFE-17-06812.

[36] L. Haferkamp, A. Spierings, M. Rusch, D. Jermann, M.A. Spurek, K. Wegener, Effect of Particle size of monomodal 316L powder on powder layer density in powder bed fusion, Prog. Addit. Manuf. 6 (3) (2021) 367–374, http://dx.doi.org/10.1007/s40964-020-00152-4.

[37] A. Rosato, K.J. Strandburg, F. Prinz, R.H. Swendsen, Why the Brazil nuts are on top: Size segregation of particulate matter by shaking, Phys. Rev. Lett. 58 (10) (1987) 1038–1040, http://dx.doi.org/10.1103/PhysRevLett.58.1038.

Kai Drechsel is a graduate at Karlsruhe Institute of Technology and received both his bachelor's and his master's degree in mechanical engineering at KIT. After graduating, he began working at the wbk - Institute of Production Science in the research group of Prof. Dr.-Ing. habil. Volker Schulze and Prof. Dr.-Ing. Frederik Zanger. For his doctoral thesis he focuses on the experimental and simulative development of an ultrasonically excited recoating process in laser powder bed fusion and the processing of fine, agglomerating 316L powder under the supervision of Prof. Dr.-Ing. habil. Volker Schulze.

Victor Lubkowitz graduated from the UAS Stralsund with a bachelor's and from Coburg with a master's degree in mechanical engineering. After graduation, he started

working at wbk - Institute of Production Science in the research group of Prof. Dr.-Ing. habil. Volker Schulze and Prof. Dr.-Ing. Frederik Zanger. For his doctoral thesis under supervision of Prof. Dr.-Ing. habil. Volker Schulze, he focuses on metal–matrix composites. Thereby fine B4C particles are mixed with an aluminum powder to a non flowable feedstock which is processed in a laser powder bed fusion process to increase the mechanical properties of the new material.

Lena Albrecht is a graduate at Karlsruhe Institute of Technology and received both her bachelor's and her master's degree in mechanical engineering at KIT. In her master's studies she initially focused on medical technology and fluid dynamics. Due to her job as a student research assistant at the Institute of Fluid Dynamics, she got in touch with additive manufacturing used for structural drag reduction. After developing a strong interest and enthusiasm about additive manufacturing, her journey led to the Institute of Production Science, where she composed her master's thesis and participated in further research focusing on laser-based powder bed fusion.

Paul Schäfer studies in Mechanical Engineering at Karlsruhe Institute of Technology. In his Bachelor Thesis he did research on the visual analysis of Powder Layers in PBF-LB process with use of machine learning algorithms.

Markus Schneider studied Mechanical Engineering at University Karlsruhe (TH) and also received his PHD there. During his studies he gained experience in automated and robot-assisted production technologies as well as simulation driven product development. After his university career he worked for several years in the Corporate Research Department of ABB AG, where he developed next generation switching technologies for medium and high voltage applications. Since 2019 he is heading the Research and Development activities at PP-Tech Components GmbH, investigating new technology applications for ultrasonic equipment.

Volker Schulze studied Mechanical Engineering at University Karlsruhe (TH). He received his PHD there in materials technology and worked as Postdoc on mechanical surface and heat treatments. Since 2008 he is one of the directors of wbk Institute of Production Science and also one of the directors of the Institute of Applied Materials at Karlsruhe Institute of Technology. His fields of interests are now mainly manufacturing technologies like cutting and additive manufacturing processes.

Frederik Zanger is an experienced manufacturing engineer in additive manufacturing, machining of metals, simulation of manufacturing processes, and digitalization of process chains. He has established the research group Additive Manufacturing at wbk Institute of Production Science at Karlsruhe Institute of Technology (KIT). As one of the directors of the institute, he holds the chair for digitalization of process development for additive manufacturing since 07/2023. His expertise in additive manufacturing is on powder bed fusion (metals), directed energy deposition (metals), binder jetting (metals) and vat photopolymerization (ceramics) processes.